CI&CEQ
Chemical Industry & Chemical Engineering Quarterly

Available online at
Association of the Chemical Engineers of Serbia AChE
www.ache.org.rs/CICEQ
Chem. Ind. Chem. Eng. Q. 33 (2) xxx–xxx (2027) CI&CEQ

ALAA A. BAHAT
https://orcid.org/0009-0009-5465-4775
WAFAA K. MAHMOOD
https://orcid.org/0000-0002-8919-2920
SAMAR S. HUSSEIN
https://orcid.org/0000-0002-0073-849X

Department of Mining and Extractive Metallurgy Engineering, College of Production Engineering and Metallurgy, University of Technology, Iraq

SCIENTIFIC PAPER

UDC

COMPARATIVE BIOSORPTION OF LEAD (II) USING *Saccharomyces cerevisiae* AND NANOCARBON-ALGINATE BEADS

Highlights

- Compared yeast-alginate and nanocarbon-alginate beads for Pb (II) biosorption from water
- Yeast-alginate beads removed 37.65% of Pb (II) at 50 mg/L within 60 minutes
- Nanocarbon-alginate beads reached 45.76 mg/g capacity at 500 mg/L Pb (II)
- Pseudo-second-order kinetics confirmed chemisorption controls all sorbent systems
- Sorbent loading (0.6 vs 0.8 g) shifted isotherms from Langmuir to Freundlich behavior

Abstract

Pb (II) removal from aqueous solution was studied with two immobilized sorbents, Saccharomyces cerevisiae-alginate beads and nanocarbon-alginate beads (nanocarbon is multi-walled carbon nanotube, MWCNT). Beads containing 0.6 or 0.8 g of sorbent were contacted with Pb (II) solutions at nominal concentrations of 50, 100, 300, and 500 mg/L (AAS-measured 58.1, 102.8, 323.0, and 496.0 mg/L). Yeast-alginate beads were more effective in dilute solution, with 37.65% removal within 5 min at 50 mg/L (0.8 g loading). The 0.8 g nanocarbon beads showed the highest apparent capacity at 500 mg/L (45.76 mg/g), since uptake had not plateaued by 60 min. The pseudo-second-order model described the kinetic data better than the pseudo-first-order model in 8 of 12 nonlinear fits, consistent with but not indicative of a chemisorption-limited rate step. The 500 mg/L data were excluded from modeling because the fits were poor or physically uninterpretable. From 50 to 300 mg/L, nonlinear fitting favored the Langmuir model for 0.6 g yeast and 0.8 g carbon and the Freundlich model for 0.8 g yeast and 0.6 g carbon, so the expected shift with loading appeared for yeast only. Yeast-alginate beads suit dilute Pb (II) streams and nanocarbon-alginate beads suit concentrated streams.

Keywords: adsorption isotherms; adsorption kinetics; biosorption; dosage-dependent adsorption; immobilized beads.

INTRODUCTION

Lead is one of the most persistent toxic metals in contaminated water and industrial effluents [1, 2]. Pb (II) is not removed by biological or chemical processes for many organic pollutants under normal environmental conditions. It may persist for long periods of time once released into aquatic systems. It is associated with suspended solids and sediments, and enters living systems by way of drinking and irrigation water and food chain transfer. Lead exposure has been associated with neurological problems, renal effects, haematological changes, and developmental disorders, and children are especially vulnerable to these toxic effects [1,2]. Therefore, the removal of Pb (II) from polluted aqueous streams remains a considerable challenge to environmental treatment and water quality protection. Lead contamination can come from various sources, but industrial activities are among the most important drivers. Wastewater with Pb (II) concentrations much higher than those usually found in drinking-water systems can be generated by battery production and recycling, metal plating, mining and smelting, pigment production, ceramic production, and improper disposal of lead-containing waste [3]. High-strength effluent treatment systems are usually evaluated in terms of discharge limits achieved, but also in terms of adsorptive capacity and rate, ease of operation, and possibility of sorbent material recovery or recycling [3]. During the last decades, many conventional methods have been studied and tested to

Correspondence: Wafaa K. Mahmood, Department of Mining and Extractive Metallurgy Engineering, College of Production Engineering and Metallurgy, University of Technology-Iraq, Baghdad, Iraq.
Email: wafaa.k.mahmood@uotechnology.edu.iq
Paper received: 24 July 2026
Paper revised: 8 October 2026
Paper accepted: 13 October 2026
https://doi.org/10.2298/CICEQ260724014B

remove lead and other heavy metals from wastewater [4–7]. Chemical precipitation is commonly used because it is economically feasible, but it produces large volumes of metal-rich sludge and may have poorer performance when low residual concentrations are required. Ion exchange has good removal performance but is highly dependent on the presence of competing ions. Membrane processes like reverse osmosis and nanofiltration are effective, but they are associated with high operating and maintenance costs [4-7]. Biosorption has received considerable attention as a low-cost alternative method for the removal of metals [8-12]. Metal ions can be incorporated into biological material mainly by reaction with the functional groups on the surface of the biomass and can occur even when the biomass is metabolically inactive. This is a practical advantage as the sorbent need not be viable during the treatment. The biosorbents for Pb (II) can act through electrostatic attraction, ion exchange, surface complexation, chelation, and sometimes microprecipitation on or near the surface of biomass [8-12]. The biosorption performance depends on the type of sorbent, the concentration of solution, contact time, pH, and the amount of sorbent [13-17]. This is because these mechanisms rely on the surface chemistry and the availability of functional groups. The presence of several biopolymers in its cell wall, such as glucans, mannoproteins, and chitin, makes *Saccharomyces cerevisiae* (baker's yeast) a low-cost potential biosorbent. These biopolymers have the ability to bind metal ions on their surfaces with carboxyl, hydroxyl, phosphate, amino, and sulfhydryl groups, which have different binding mechanisms [18,19]. Carbon materials at macro-, micro-, and nano-scales have also been studied as cost- and performance-effective adsorption agents, but a constant disadvantage of carbon-based adsorbents, especially nanocarbon powders, is recovery and regeneration, which can increase operating cost and create technical difficulties such as clogging, poor media distribution, and agglomeration [18,20]. To overcome these drawbacks, many groups immobilised the adsorbents in biopolymer beads [21-23]. Sodium alginate, a naturally occurring anionic polysaccharide, is one of the most common supports for this purpose and forms hydrogels upon cross-linking with calcium ions. Immobilisation of adsorbents in alginate hydrogels and the formation of beads of controlled sizes directly address some of the handling difficulties associated with fine or nano-scale sorbents, since the beads are easier to separate from treated water and flow more predictably in flow systems [21-23]. It is also possible to combine more than one adsorption agent in one uniformly distributed composite sorbent by using alginate beads, which provides a useful degree of flexibility for designing new biosorbents.

In this work, the removal of Pb (II) by two adsorption agents, namely *S. cerevisiae* and nano-carbon (multi-walled carbon nanotubes, MWCNTs), was studied. Each of these agents was immobilised separately in sodium alginate and prepared as beads of uniform size. The variables studied were the concentration of Pb (II), contact time, and amount of sorbent added during bead preparation. Batch biosorption experiments were carried out to evaluate the effect of these variables on removal efficiency and adsorption capacity. The experimental data were fitted to the pseudo-first-order and pseudo-second-order kinetic models by using nonlinear regression with explicit error statistics. The pseudo-second-order model was also fitted in linear form for comparing the two approaches. To test if sorbent identity and loading were associated with different equilibrium behaviour, Langmuir and Freundlich isotherm models were also fitted non-linearly to capacity trends at apparent equilibrium. The kinetic and equilibrium patterns are discussed as observations consistent with particular families of models, not as direct proof of a particular molecular mechanism. The points at which the present data cannot distinguish between competing explanations are identified explicitly.

MATERIALS AND METHODS

Materials and Biosorbent Preparation

In the present work, the main materials used are Baker's yeast (*S. cerevisiae*, commercial, viability >95%), sodium alginate (MW ≈ 200 kDa), calcium chloride dihydrate ($CaCl_2 \cdot 2H_2O$, purity >99%), and lead (II) nitrate ($Pb(NO_3)_2$, purity >99%), which were purchased from Sigma-Aldrich. Also, Multi-walled carbon nanotubes (MWCNTs; average diameter of 10 to 15 nm, length of 1 to 10 μm, purity >95%) were supplied by Sigma-Aldrich.

All solutions were prepared with double-distilled deionized water (>18 MΩ cm resistivity). To prepare the yeast-alginate beads, dry yeast was first inactivated by autoclaving at 121 °C, 15 psi for 30 min, which makes the functional groups buried in the cell wall more accessible. Sodium alginate (4.0 g) was dissolved in 200 mL of water, and autoclaved yeast (0.6 or 0.8 g) was stirred gently into the solution [21,24,25].

Nanocarbon-alginate beads were prepared by ultrasonically dispersing the nanocarbon (0.6 or 0.8 g) directly in the alginate solution for 15 min, which led to a more even dispersion. For both sorbents, the dispersion was extruded dropwise into 500 mL of $CaCl_2$ solution and cured for 45 min. The beads were washed three times with distilled water and stored at 4 °C. The $CaCl_2$ concentration, extrusion needle size, bead diameter, and size distribution were not recorded. These factors influence external mass transfer and therefore the comparison of kinetic behavior between the sorbents. The values 0.6 g and 0.8 g refer to the mass of yeast or nanocarbon dispersed in 200 mL alginate solution in bead preparation. They do not specify the mass of active sorbent in the 1.0 g of wet beads added to each adsorption flask. On a dry precursor basis (sorbent mass relative to the total dry mass of sorbent and alginate, prior to water uptake during gelation and curing), the 0.6 g loading is approximately 13.0% of the dry solids, and the 0.8 g loading is approximately 16.7%. The wet mass of the beads was not recorded, so the exact mass of active agent per gram of wet bead is not known. Hence, all adsorption capacities (q_e) in the present work are given per gram of wet bead, in accordance with Eq. (2), and should not be read as capacities per gram of yeast or nanocarbon alone.

No alginate-only (blank bead) control was run. Calcium alginate binds divalent metal ions by ion exchange at its

guluronate residues, so part of the reported Pb (II) uptake for both sorbent systems may be due to the alginate matrix and not specifically to the yeast or nanocarbon. The removal efficiencies and capacities reported here therefore describe whole beads and not the yeast or nanocarbon alone.

Biosorption experiments

A stock Pb (II) solution of 1000 mg/L was prepared by dissolving $Pb(NO_3)_2$ in deionized water. Working solutions with nominal concentrations of 50, 100, 300 and 500 mg/L were prepared by serial dilution of the stock solution. The initial Pb (II) concentrations determined experimentally by AAS were 58.1, 102.8, 323.0 and 496.0 mg/L, respectively. All the removal efficiency (R%) and adsorption capacity (q_e) reported were calculated from these measured values instead of nominal ones. The nominal values (50, 100, 300, and 500 mg/L) serve as mere labels for the four treatment levels.

Batch biosorption experiments were carried out in 1 L flasks containing 1.0 g wet beads and 500 mL Pb (II) solution, shaken at 150 rpm and 21-23 °C. The pH of the solution was not measured or controlled. Because pH strongly affects Pb (II) speciation and the likelihood of hydrolysis or surface precipitation, especially at the higher concentrations tested, a contribution from pH-related precipitation to the measured removal cannot be excluded. All removal and capacity values are therefore reported as net loss of Pb (II) from solution and not as adsorption in the strict mechanistic sense.

At t = 1, 5, 30, and 60 min, samples of 5 mL were taken from each run. They were filtered through a 0.45 μm PTFE membrane, diluted 1 to 10 with 2% HNO_3, and analyzed by AAS at 283.3 nm, with reagent blanks included for quality control. The measurements were made in triplicate, and the mean values are reported in Table 1, with Tables 2 and 3 giving parameters derived from them. Standard deviations are not reported because the individual replicate readings were not retained. The total volume withdrawn by sampling (4 × 5 mL, 4% of the initial volume) was neglected, and V was taken as constant at 0.5 L.

Taken together, the absence of pH data, of an alginate-only control, of retained replicate readings, and of recorded bead dimensions limits the conclusions to the comparative performance of whole beads under the stated conditions. These data do not allow the removal mechanism to be identified. Future work should include pH monitoring and control, an alginate-only control, additional kinetic time points, retained replicate-level data, and recorded bead dimensions.

Kinetic and Isotherm Analysis

The Pb (II) removal efficiency was calculated as follows:

$$R\% = \left[\frac{((C_i - C_f)}{C_i}\right] \cdot 100 \qquad (1)$$

where R% is the removal efficiency, C_i is the initial Pb (II) concentration (AAS-measured), and C_f is the final Pb (II) concentration.

The adsorption capacity was calculated as follows:

$$q_t = (C_i - C_t)V/m \qquad (2)$$

where V = 0.5 L, m = 1 g (mass of wet beads), and q_t is the adsorption capacity at time t.

The linearized pseudo-second-order (PSO) model is given as follows:

$$t/q_t = 1/(k_2\, q_e^2) + t/\, q_e \qquad (3)$$

where k_2 is the pseudo-second-order rate constant (g mg^{-1} min^{-1}).

The linearized PFO form requires an independent estimate of q_e, which is not available for systems that have not plateaued by 60 min, so only the PSO model was linearized. Both the pseudo-first-order ($q_t = q_e\,[1 - \exp(-k_1 t)]$) and pseudo-second-order ($q_t = k_2\, q_e^{\,2} t / (1 + k_2\, q_e t)$) equations were fitted directly to the raw q_t-versus-t data by nonlinear least-squares regression, because linearized R^2 values alone can overstate model fit, particularly with a small number of time points. For each fit, the calculated equilibrium capacity (q_e, cal), the rate constant, the nonlinear R^2, and the root-mean-square error (RMSE) are reported, and q_e, cal is compared with the experimental q_e at 60 min ($q_{e,exp}$). Both the linearized and the nonlinear kinetic analyses rest on only four time points (1, 5, 30, and 60 min), which limits the precision with which the two models can be statistically discriminated.

For the equilibrium isotherms, the linearized Langmuir model is given as follows:

$$C_e/q_e = C_e/q_{max} + 1/(K_L\, q_{max}) \qquad (4)$$

where C_e is the equilibrium Pb (II) concentration (mg/L), q_{max} is the maximum monolayer adsorption capacity (mg/g), and K_L is the Langmuir equilibrium constant (L/mg).

The linearized Freundlich model is given as follows:

$$\log(q_e) = \log(K_F) + (1/n)\, \log(C_e) \qquad (5)$$

where K_F is the Freundlich adsorption constant ((mg/g)(mg/L)$^{-1/n}$), and n is the Freundlich intensity factor (dimensionless).

The Langmuir separation factor is given as follows:

$$R_L = 1/(1 + K_L\, Ci) \qquad (6)$$

where R_L is a dimensionless constant; $0 < R_L < 1$ indicates favorable adsorption.

As with the kinetic data, the Langmuir and Freundlich isotherms were also fitted directly to the C_e-q_e pairs by nonlinear regression ($q_e = q_{max}\, K_L\, C_e/(1 + K_L\, C_e)$ for Langmuir and $q_e = K_F\, Ce^{1/n}$ for Freundlich). Values of q_{max} and K_L (or K_F and n), together with the nonlinear R^2 and RMSE, are reported for every system. The isotherm analysis uses the equilibrium (60 min) q_e values from the 50, 100, and 300 mg/L treatments. The 500 mg/L data were excluded from both the kinetic and the isotherm nonlinear fitting, and the quantitative justification for this exclusion is given in the Results and Discussion section.

RESULTS AND DISCUSSION

Effect of contact time on removal efficiency and adsorption capacity

Fig. 1 shows the removal efficiency (R%) versus contact time for four initial Pb (II) concentrations (50, 100, 300, and 500 mg/L). At 50 mg/L (Fig. 1a), R% for 0.8 g yeast-alginate was 37.65% after 5 min and remained above

34% through 60 min, while the 0.6 g systems equilibrated more slowly and reached 24 to 27% by 60 min. For most systems at higher concentrations (Fig. 1c, d), *R*% decreased markedly. Three systems fell below 10% (0.6 g yeast, 3.00%; 0.8 g yeast, 9.27%; 0.6 g carbon, 5.04%) at 500 mg/L, while 0.8 g carbon increased to 18.45%, the highest *R*% of any system at this concentration. Because no replicate data are reported, this reversal is treated as an observation that cannot be confirmed to exceed normal experimental scatter, and not as evidence of a separate mechanism. In general, yeast systems showed a rapid early uptake that plateaued by 30 min, while carbon systems showed a more gradual uptake that in several cases had not clearly plateaued by 60 min. Thus, the 60 min values for the carbon systems are considered in the present work as apparent, not confirmed, equilibrium capacities.

The corresponding adsorption capacity (q_e) in the same period of time is shown in Fig. 2. The yeast systems ramp up sharply from 1 to 5 min, reaching a plateau by 30 min [26], while the carbon systems increase more slowly over 60 min, consistent with slower diffusion into the porous nanocarbon structure [27]. This pattern is consistent with a diffusion-limited uptake step for the carbon systems but not conclusive evidence of a particular binding mechanism since contact-time behavior alone cannot distinguish diffusion control from surface-reaction control.

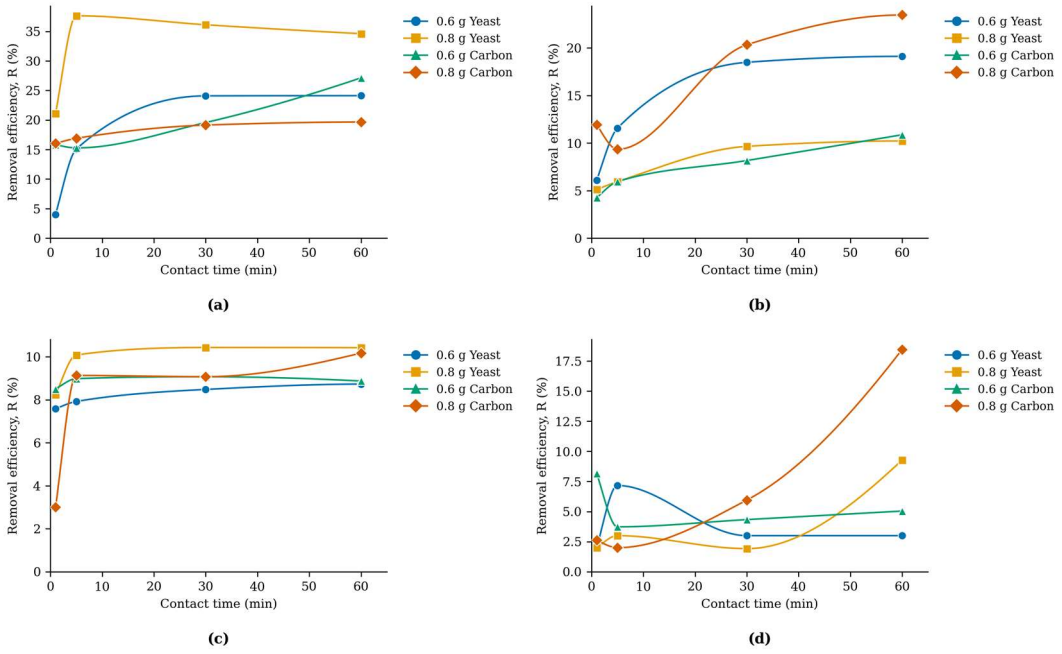


Figure 1. Removal efficiency (R%) vs. contact time at four initial Pb concentrations: a) 50 mg/L, b) 100 mg/L, c) 300 mg/L, and d) 500 mg/L.

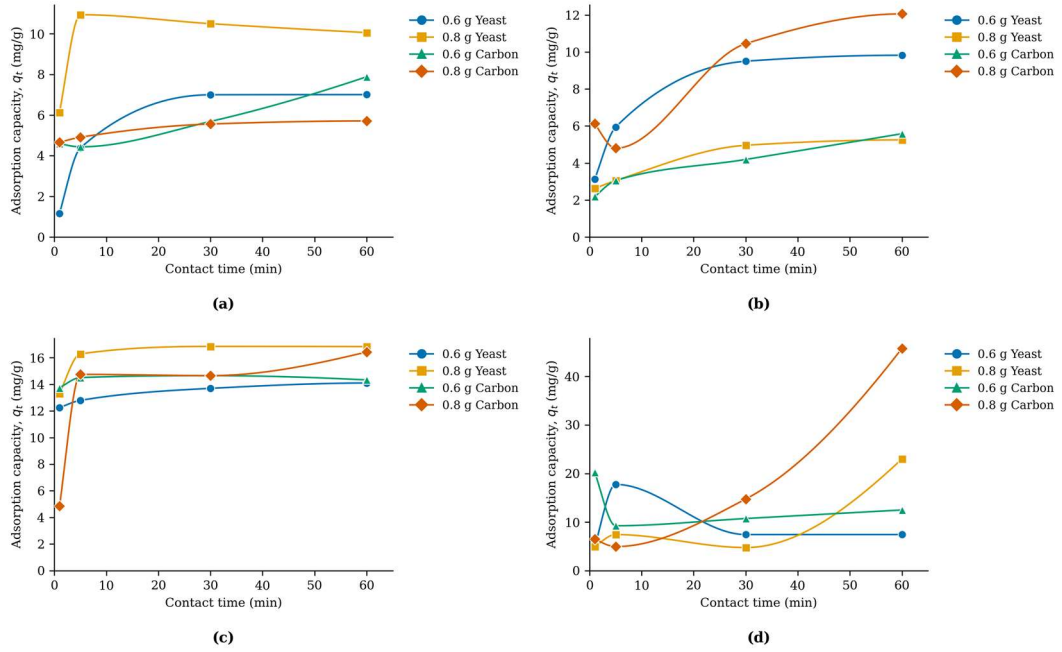


Figure 2. Adsorption capacity (q_e, mg/g) vs. contact time: a) 50 mg/L, b) 100 mg/L, c) 300 mg/L, and d) 500 mg/L.

Effect of initial concentration on removal efficiency and adsorption capacity

Table 1 shows the R% and q_e at 60 min for the four systems at all four concentrations. At 50 mg/L, R% at 60 min varied from 19.66% (0.8 g carbon) to 34.62% (0.8 g yeast). At 500 mg/L, R% varied from 3.00% (0.6 g yeast) to 18.45% (0.8 g carbon), such that 0.8 g carbon was the exception noted above, with the highest rather than the lowest R% of the four systems. For 0.6 g carbon, R% decreased from 27.14% at 50 mg/L to 5.04% at 500 mg/L, a range of 5 to 27%. The adsorption capacity (q_e) generally increased with concentration, but not for every system. For 0.6 g yeast, q_e increased from 7.01 mg/g at 50 mg/L to a maximum of 14.10 mg/g at 300 mg/L and then decreased to 7.44 mg/g at 500 mg/L, and q_e for 0.6 g carbon was also non-monotonic (7.89, 5.58, 14.33 and 12.50 mg/g at 50, 100, 300 and 500 mg/L). In contrast, q_e for 0.8 g carbon increased steadily with concentration from 5.71 mg/g at 50 mg/L to 45.76 mg/g at 500 mg/L, and 0.8 g yeast overall increased from 10.06 to 22.99 mg/g despite a drop to 5.25 mg/g at 100 mg/L. The non-monotonic behavior at 0.6 g loading and at 100 mg/L cannot be explained from the available data, and without replicate data it is not possible to tell whether these deviations lie within normal measurement scatter. They are treated as unexplained variability and not as evidence for or against any adsorption mechanism.

A direct comparison between the two loadings shows that the 0.8 g systems generally achieved higher capacities than the corresponding 0.6 g systems, consistent with more sorbent sites available at the higher loading. However, 0.6 g loading is not simply a scaled-down version of 0.8 g loading in terms of composition (Materials and Methods). The q_e dependence on concentration was much stronger for 0.8 g carbon (about an 8-fold increase from 50 to 500 mg/L) than for 0.6 g yeast (about up to 2.0-fold change over the same range, depending on which concentrations are compared). The isotherm modeling subsection below examines whether this difference is best explained by a change in the underlying shape of the isotherm following the kinetic analysis.

Dosage comparison within each sorbent type

The yeast systems followed a similar trend for the 0.6 g and 0.8 g loadings, with *R%* decreasing from the 24 to 35% range at 50 mg/L to the 3 to 9% range at 500 mg/L. This similarity suggests that the fundamental removal mechanism is not qualitatively affected by yeast loading, although this cannot be confirmed independently of the kinetic and isotherm modeling discussed below. The carbon systems became more divergent with loading. *R%* for 0.6 g carbon decreased from 27.14% to 5.04% over the concentration range, whereas 0.8 g carbon increased from 10.17% at 300 mg/L to 18.45% at 500 mg/L, reversing the declining trend shown by every other system. The major empirical pattern motivating the isotherm comparison that follows is this non-monotonic, loading-dependent behavior of the carbon systems. This is treated as an observation to be examined by modeling rather than as proof of a mechanistic change.

Table 1. Removal Efficiency R% and Adsorption Capacity q_e (mg/g) at 60 min.

Biosorbent	Dosage (g)	R% (50 mg/L)	q_e (50 mg/L)	R% (100 mg/L)	q_e (100 mg/L)	R% (300 mg/L)	q_e (300 mg/L)	R% (500 mg/L)*	q_e (500 mg/L)*
Yeast	0.6	24.12	7.01	19.12	9.82	8.73	14.10	3.00	7.44
Yeast	0.8	34.62	10.06	10.22	5.25	10.42	16.83	9.27	22.99
Carbon	0.6	27.14	7.89	10.87	5.58	8.87	14.33	5.04	12.50
Carbon	0.8	19.66	5.71	23.47	12.06	10.17	16.43	18.45	45.76

Kinetic modeling with linearized PSO and nonlinear PFO and PSO fits

Modeling of the experimental data is included for two reasons. Kinetic modeling condenses the time dependence of uptake into a small number of comparable parameters (the calculated q_e and the rate constants), and isotherm modeling does the same for the dependence of capacity on concentration. Both allow the two sorbents and the two loadings to be compared quantitatively with each other and with other studies, and they show how closely each model family describes the data, without being treated as proof of a molecular mechanism.

Fig. 3 shows the linearized pseudo-second-order (PSO) plots (t/q_t vs. t) for the 50, 100, and 300 mg/L treatments. The 500 mg/L data were not used for the linearized kinetic fits. Recalculated from the mean q_t values, the linearized PSO fits gave R^2 between 0.963 and 1.000 and k_2 between 0.0153 and 0.2887 g/(mg·min) (Table 2). Two combinations (0.8 g yeast at 50 mg/L and 0.6 g carbon at 300 mg/L) gave a negative intercept, so k_2 is not defined for them. Because a t/q_t plot built from four points is dominated by the long-time points, a high linear R^2 does not discriminate between the kinetic models, and the nonlinear comparison below carries the model assessment.

Because a kinetic analysis based on only four time points, with a wide gap between 5 and 30 min, limits how confidently the PFO and PSO models can be discriminated statistically, both models were also fitted directly to the raw qt-t data by nonlinear least-squares regression. The resulting q_e, cal, rate constants, nonlinear R^2, and RMSE are reported in Table 2 alongside the experimental q_e at 60 min (q_e, exp). For the 50, 100, and 300 mg/L treatments, both models generally converged to physically reasonable parameters. The nonlinear PSO fit gave q_e, cal within about 10% of q_e, exp for eleven of the twelve system-concentration combinations, and the nonlinear PSO R^2 was higher than the nonlinear PFO R^2 in eight of the twelve. This gives a modest preference for the PSO model. The PFO model fitted equally well or better for 0.6 g yeast and 0.8 g yeast at 50 mg/L and for the two carbon systems at 300 mg/L.

At 500 mg/L, by contrast, the nonlinear kinetic fits were not usable. For 0.6 g yeast, the nonlinear R^2 values were poor (0.233 for PFO and 0.090 for PSO), and for 0.6 g carbon, both models gave an R^2 of approximately zero, reflecting the non-monotonic q_t–t trend at this concentration

(Fig. 2d). For 0.8 g yeast and 0.8 g carbon, the optimizer converged only to degenerate parameter combinations in which the rate constant approached zero. The calculated equilibrium capacities reached 345,653 and 711,317 mg/g for the PFO model and 5,957 and 8,596 mg/g for the PSO model (0.8 g yeast and 0.8 g carbon, respectively), between two and four orders of magnitude above the highest experimentally observed q_e for these systems. Such parameter values are not physically meaningful and indicate that the fitted curve approximates a near-linear trend rather than a genuine saturating kinetic process. This is the quantitative basis for excluding the 500 mg/L data from kinetic (and, below, isotherm) modeling, because at this concentration the available data do not support stable, physically interpretable PFO or PSO parameter estimates, independently of the removal percentage itself. The 500 mg/L removal and capacity values are retained in Table 1 as observed data, since the measurements themselves are not in question, but they are not used to draw kinetic or equilibrium model conclusions.

The generally better PSO fit, where it holds, is consistent with a rate-limiting step that depends on the availability of binding sites rather than on the bulk-solution Pb (II) concentration alone, a pattern traditionally associated with chemisorption-type kinetics in the biosorption literature [28-30]. The PSO fit is not, however, direct proof of chemisorption, electron transfer, or chelation, since kinetic model fitting alone cannot distinguish a genuinely chemical rate-limiting step from one governed by other factors such as pore or site saturation. Independent spectroscopic or surface-chemical evidence (for example, FTIR before and after Pb (II) loading) would be needed to support a specific molecular mechanism, and such evidence was not collected for this study.

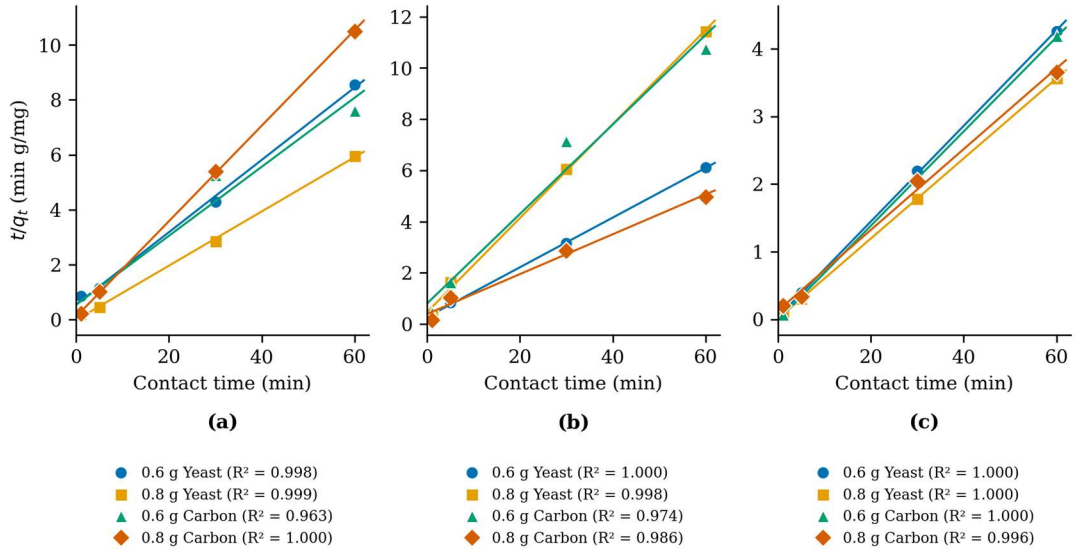


Figure 3. Pseudo-second-order (PSO) kinetics, t/q_t vs. contact time: a) 50 mg/L, b) 100 mg/L, and c) 300 mg/L.

Table 2. Kinetic parameters from linearized PSO fits (50 to 300 mg/L), and nonlinear PFO and PSO fits with error statistics.

Biosorbent	Conc. (mg/L)	q_e, exp (mg/g)	Linear PSO q_e, cal	Linear PSO k2	Linear PSO R^2	NL PFO q_e, cal	NL PFO k_1	NL PFO R^2	NL PFO RMSE	NL PSO q_e, cal	NL PSO k_2	NL PSO R^2	NL PSO RMSE
0.6 g Yeast	50	7.01	7.600	0.0313	0.998	7.019	0.1935	1.000	0.040	7.743	0.0308	0.990	0.241
0.6 g Yeast	100	9.82	10.312	0.0336	1.000	9.588	0.2279	0.942	0.665	10.273	0.0327	0.981	0.377
0.6 g Yeast	300	14.10	14.149	0.1491	1.000	13.528	2.3524	0.581	0.474	13.720	0.5493	0.759	0.359
0.8 g Yeast	50	10.06	10.128	n.d.	0.999	10.525	0.8901	0.965	0.358	10.879	0.1435	0.833	0.784
0.8 g Yeast	100	5.25	5.449	0.0717	0.998	4.892	0.3400	0.524	0.792	5.057	0.1354	0.775	0.544
0.8 g Yeast	300	16.83	16.901	0.2887	1.000	16.653	1.5992	0.977	0.225	17.011	0.2132	0.996	0.097
0.6 g Carbon	50	7.89	7.962	0.0291	0.963	6.013	1.4285	0.197	1.234	6.447	0.2657	0.377	1.087
0.6 g Carbon	100	5.58	5.726	0.0378	0.974	4.771	0.2946	0.643	0.762	5.038	0.0971	0.794	0.578
0.6 g Carbon	300	14.33	14.350	n.d.	1.000	14.492	2.9422	0.893	0.114	14.553	1.1823	0.847	0.137
0.8 g Carbon	50	5.71	5.755	0.2717	1.000	5.396	1.9929	0.527	0.301	5.520	0.8678	0.726	0.230
0.8 g Carbon	100	12.06	12.858	0.0153	0.986	11.137	0.1752	0.358	2.394	11.335	0.0363	0.515	2.080
0.8 g Carbon	300	16.43	16.756	0.0275	0.996	15.763	0.4332	0.967	0.835	16.764	0.0360	0.900	1.443

Isotherm modeling and the distinction between fitted q_{max} and experimental $q_{e,max}$

Table 3 reports only regression-derived parameters, namely q_{max} and K_L from nonlinear Langmuir fitting and KF and n from nonlinear Freundlich fitting, for every system, fitted to the equilibrium (60 min) C_e-q_e pairs at 50, 100, and 300 mg/L. As in the kinetic analysis, the 500 mg/L point was excluded from isotherm fitting. The experimental maximum qe values from Table 1 are listed in a separate column of Table 3 for reference and are not Langmuir q_{max} values.

Fig. 4 shows the linearized Langmuir plots (C_e /q_e vs. C_e) and Fig. 5 shows the linearized Freundlich plots (log(q_e) vs. log(C_e)) for the three concentrations used in

modeling, and Table 3 reports the nonlinear fit statistics. Because only three equilibrium concentrations were available, each two-parameter isotherm model is fitted with only one degree of freedom. Nonlinear R^2 values close to 1 under these conditions, as for 0.6 g yeast, should therefore be interpreted cautiously, and RMSE is reported alongside R^2 so that the quality of each fit can be judged independently.

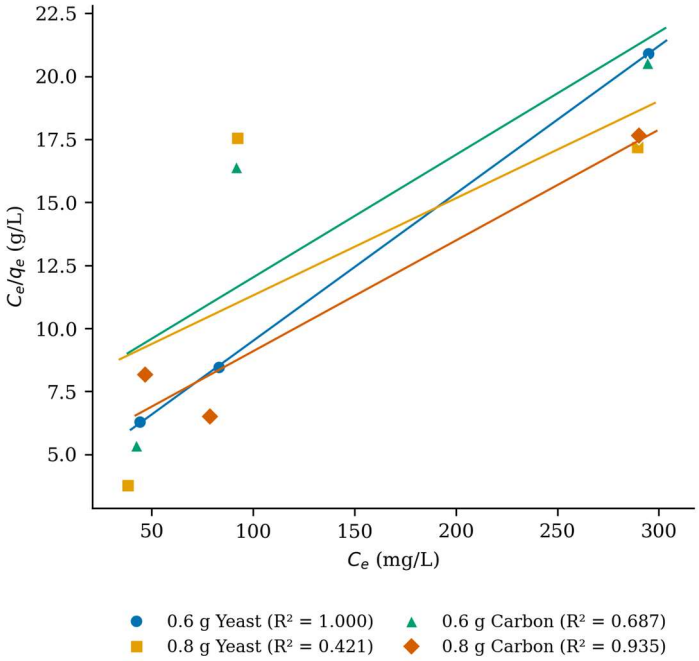


Figure 4. Langmuir isotherms, C_e/q_e versus equilibrium concentration (50 to 300 mg/L).

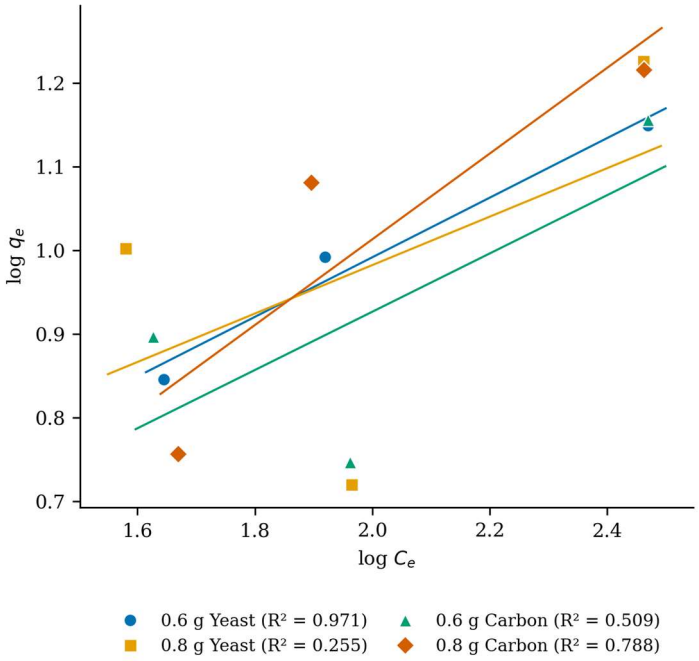


Figure 5. Freundlich isotherms, log(q_e) versus log(C_e) (50 to 300 mg/L).

Under nonlinear fitting, the comparison of Langmuir and Freundlich performance does not follow a simple pattern of Langmuir behavior at 0.6 g loading and Freundlich behavior at 0.8 g loading for both sorbents. Both models provide a good fit to the data for 0.6 g yeast (nonlinear R^2 of 1.000 for Langmuir and 0.979 for Freundlich), which is consistent with, but not diagnostic of, monolayer-type behavior at this loading. The single degree of freedom noted above makes this at best a weak preference. The fit of Freundlich was moderately better than Langmuir for 0.8 g yeast and 0.6 g carbon (R^2 of 0.520 vs. 0.366 for 0.8 g yeast and 0.722 vs. 0.606 for 0.6 g carbon). The nonlinear Langmuir fit (R^2 = 0.886) was better than the nonlinear Freundlich fit (R^2 = 0.827) for 0.8 g

carbon. Therefore, no established finding is presented of a clean, dosage-driven transition from Langmuir to Freundlich behavior. Only the two yeast systems follow this pattern, and neither carbon system does. This mixed, system-specific outcome is presented as such, not as confirmation of a general mechanistic rule. In the future, any mechanistic claim for these systems should be supported by independent surface-characterization evidence rather than by comparing isotherm models alone.

The separation factor R_L (Eq. 6) based on the refitted Langmuir K_L values is between 0 and 1 for all four systems over the modeled concentration range (0.52 to 0.67 at 50 mg/L and 0.16 to 0.27 at 300 mg/L), indicating favorable adsorption for all systems under this model.

Fig. 6 compares the four systems in terms of three integrated metrics, namely the maximum experimentally observed adsorption capacity, the removal efficiency at the lowest tested concentration, and the q_e, 500/q_e, 50 ratio as a simple metric of concentration sensitivity. The q_e, 500 values in this ratio are from the excluded 500 mg/L treatment and are descriptive of the data, not inputs to the fitted isotherms. The highest maximum observed q_e was found for 0.8 g carbon (45.76 mg/g at 500 mg/L), followed by 0.8 g yeast (22.99 mg/g), 0.6 g carbon (14.33 mg/g at 300 mg/L), and 0.6 g yeast (14.10 mg/g at 300 mg/L). The removal efficiency was highest for 0.8 g yeast (34.62%) at the lowest concentration tested (50 mg/L) and lowest for 0.8 g carbon (19.66%), and the ordering is reversed at high concentration. The q_e, 500/q_e, 50 ratios were 8.01 for 0.8 g carbon, 2.28 for 0.8 g yeast, 1.59 for 0.6 g carbon, and 1.06 for 0.6 g yeast, in accordance with the capacity advantage of carbon being focused at the higher end of the range tested. The yeast systems together are better for dilute Pb (II) streams, and the carbon systems, 0.8 g carbon specifically, are better for concentrated streams, although a pH-related or alginate-matrix contribution to this pattern cannot be ruled out given the limitations described in Materials and Methods.

Table 3. Nonlinear Langmuir and Freundlich isotherm parameters (fitted at 50 to 300 mg/L), with experimental maximum q_e shown separately for reference.

Biosorbent	$q_{e,max}$ experimental (Table 1, mg/g)	Langmuir					Freundlich				Better fit (this range)
		q_{max} (mg/g)	K_L (L/mg)	R^2 (NL)	RMSE	R_L range (50 to 300 mg/L)	K_F	n	R^2 (NL)	RMSE	
0.6 g Yeast	14.10 (at 300 mg/L)	17.121	0.01594	1.000	0.052	0.16 to 0.52	2.073	2.953	0.979	0.426	Langmuir (weak preference, 1 d.f.)
0.8 g Yeast	22.99 (at 500 mg/L, excluded from fit)	21.962	0.00860	0.366	3.783	0.27 to 0.67	1.342	2.306	0.520	3.291	Freundlich
0.6 g Carbon	14.33 (at 300 mg/L)	19.162	0.00846	0.606	2.323	0.27 to 0.67	1.060	2.219	0.722	1.949	Freundlich
0.8 g Carbon	45.76 (at 500 mg/L, excluded from fit)	21.981	0.01105	0.886	1.485	0.22 to 0.61	1.551	2.379	0.827	1.827	Langmuir

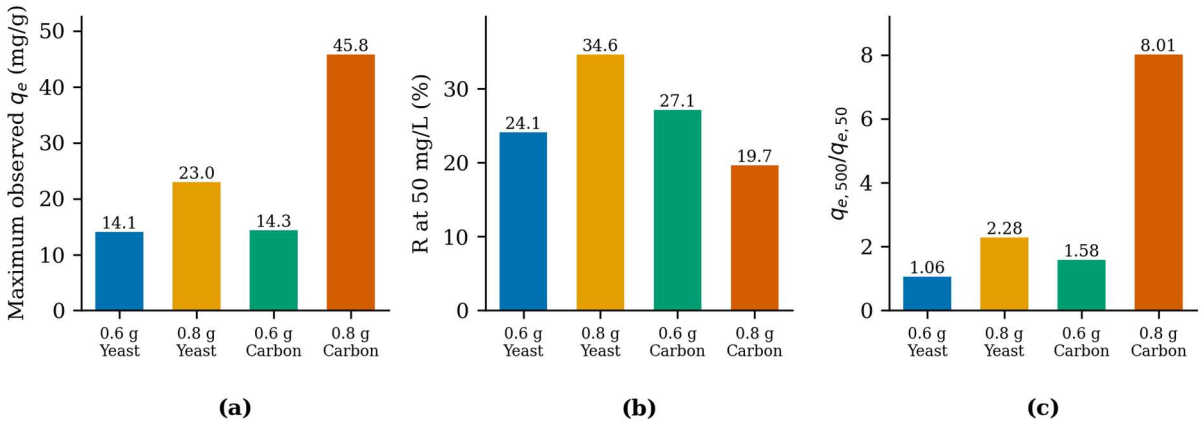


Figure 6. a) Maximum observed adsorption capacity, b) Removal efficiency at 50 mg/L, and c) $q_{e,500}/q_{e,50}$ concentration-sensitivity ratio.

CONCLUSIONS

The removal of Pb (II) at four concentrations (58.1 to 496.0 mg/L, AAS-measured) and two sorbent loadings (0.6 and 0.8 g) was compared between immobilised *S. cerevisiae*-alginate beads and nanocarbon-alginate beads. The removal efficiency of Pb (II) was 37.65% within 5 min at 50 mg/L with 0.8 g yeast beads, while the removal efficiency of 0.8 g carbon beads was 19.66% within 60 min. The highest capacity observed was 45.76 mg/g when 0.8 g carbon beads were used at 500 mg/L (compared with 22.99 mg/g for 0.8 g yeast beads), as uptake had not plateaued by 60 min. The data at 500 mg/L were not used for the fitting of kinetic or isotherm models, for the quantitative reasons discussed earlier.

In most cases under nonlinear regression (8 of 12 combinations at 50 to 300 mg/L), the pseudo-second-order model described the data better than the pseudo-first-order model, while the linearised t/qt plots (R^2 of 0.963 or higher) did not differentiate between the models. This is consistent with, but does not prove, a rate-limiting step dependent on the availability of binding sites and not on diffusion alone. Nonlinear isotherm fitting in the same concentration range gave Langmuir R^2 values of 1.000, 0.366, 0.606, and 0.886

and Freundlich R^2 values of 0.979, 0.520, 0.722, and 0.827 for 0.6 g yeast, 0.8 g yeast, 0.6 g carbon, and 0.8 g carbon, respectively. The relative fit of the two models depended on loading and sorbent type, but the data did not show a single, consistent transition from monolayer-type behaviour at low loading to multilayer-type behaviour at high loading. This pattern was only present in the two yeast systems; neither carbon system showed this. The kinetic and isotherm comparisons indicate what model of the mathematics fits the data better under the stated conditions. They are not direct evidence of the molecular mechanism. Under these conditions, yeast alginate beads are more suitable for dilute Pb (II) streams where the uptake rate is important, and nanocarbon alginate beads are more suitable for concentrated streams where the capacity is the limiting factor.

ACKNOWLEDGMENTS

The authors acknowledge the College of Production Engineering and Metallurgy, University of Technology-Iraq, for its support.

REFERENCES

[1] A.L. Caixeta, A.C.N. da Silva, S.K.S. da Silva, M. de C. Dias, C.M. Cholant, T.M. Volkmer, A.L. Missio, A.D. de Oliveira, M.M. Ferrer, Y. Anwar, S. Khan, Materials 18 (2025) 4752. https://doi.org/10.3390/ma18204752.
[2] H. Namkoong, E. Biehler, G. Namkoong, T.M. Abdel-Fattah, ACS Omega 7 (2022) 39931-39937. https://doi.org/10.1021/acsomega.2c04322.
[3] S. Ahmady-Asbchin, M. Akbari Nasab, C. Gerente, Sci. Rep. 14 (2024) 19168. https://doi.org/10.1038/s41598-024-70402-w.
[4] 4. R.Q. Alansi, A.M.A. Mohammed, M.M. Ali, W.A. Mokbel Ghalib, S.C. Ponnappa, J. Health Pollut. 11 (2021) 210604. https://doi.org/10.5696/2156-9614-11.30.210604.
[5] C.N. Mulligan, Environ. Pollut. 133 (2005) 183-198. https://doi.org/10.1016/j.envpol.2004.06.009.
[6] A. Zendelska, M. Golomeova, K. Blazev, B. Boev, B. Krstev, B. Golomeov, A. Krstev, Maced. J. Chem. Chem. Eng. 34 (2015) 213-220. https://doi.org/10.20450/mjcce.2015.552.
[7] O.K. Alduaij, M.I. Attia, L. Khezami, K.K. Taha, Maced. J. Chem. Chem. Eng. 35 (2016) 87-96. https://doi.org/10.20450/mjcce.2016.852.
[8] K. Staszak, M. Regel-Rosocka, Materials 17 (2024) 1155. https://doi.org/10.3390/ma17051155.
[9] I. Rakic, Z. Kevresan, R. Kovac, S. Kravic, Z. Svircev, A. Djurovic, Z. Stojanovic, Chem. Ind. Chem. Eng. Q. 29 (2023) 291-298. https://doi.org/10.2298/ciceq220511002r.
[10] S. Khaleel, Chem. Ind. Chem. Eng. Q. 32 (2026) 15-24. https://doi.org/10.2298/ciceq240807005k.
[11] D. Bozic, M. Gorgievski, V. Stankovic, M. Cakic, S. Dimitrijevic, V. Conic, Chem. Ind. Chem. Eng. Q. 27 (2021) 21-34. https://doi.org/10.2298/ciceq191113021b.
[12] V. Stankovic, M. Gorgievski, D. Bozic, G. Bogdanovic, Chem. Ind. Chem. Eng. Q. 28 (2022) 255-264. https://doi.org/10.2298/ciceq210617037s.
[13] N. El Messaoudi, M. El Khomri, A. El Mouden, A. Bouich, A. Jada, A. Lacherai, H.M.N. Iqbal, S.I. Mulla, V. Kumar, J.H.P. Americo-Pinheiro, Biomass Convers. Biorefin. 14 (2022) 11739-11756. https://doi.org/10.1007/s13399-022-03604-9.
[14] F. Alcalde-Garcia, S. Prasher, S. Kaliaguine, J.R. Tavares, M.-J. Dumont, ACS Eng. Au 3 (2023) 443-460. https://doi.org/10.1021/acsengineeringau.3c00022.
[15] M. Minceva, R. Fajgar, L. Markovska, V. Meshko, Sep. Sci. Technol. 43 (2008) 2117-2143. https://doi.org/10.1080/01496390801941174.
[16] Z. Yaneva, B. Koumanova, N. Georgieva, Maced. J. Chem. Chem. Eng. 31 (2012) 101-114. https://doi.org/10.20450/mjcce.2012.61.
[17] T. Arsenie, I.G. Cara, M.-C. Popescu, I. Motrescu, L. Bulgariu, Water 14 (2022) 4108. https://doi.org/10.3390/w14244108.
[18] N. Gupta, S. Arunachalam, Front. Microbiol. 16 (2025) 1647398. https://doi.org/10.3389/fmicb.2025.1647398.
[19] E. Savastru, D. Bulgariu, C.-I. Zamfir, L. Bulgariu, Water 14 (2022) 976. https://doi.org/10.3390/w14060976.
[20] N.-O. Nicula, E.-M. Lungulescu, G.A. Rimbu, V. Marinescu, V.M. Corbu, O. Csutak, Int. J. Environ. Res. Public Health 20 (2023) 4795. https://doi.org/10.3390/ijerph20064795.
[21] M. Simonic, Sustainability 16 (2024) 8174. https://doi.org/10.3390/su16188174.
[22] O. Purev, C. Park, H. Kim, E. Myung, N. Choi, K. Cho, Int. J. Environ. Res. Public Health 20 (2023) 1106. https://doi.org/10.3390/ijerph20021106.
[23] A.S.Y. Ting, K.H. Tiew, K.P. Song, Int. J. Environ. Sci. Technol. 22 (2024) 8883-8894. https://doi.org/10.1007/s13762-024-06224-0.
[24] A. De Rossi, C.V.T. Rigueto, A. Dettmer, L.M. Colla, J.S. Piccin, J. Environ. Chem. Eng. 8 (2020) 104009. https://doi.org/10.1016/j.jece.2020.104009.
[25] L. Rusu, C.-G. Grigoras, A.-I. Simion, E.-M. Suceveanu, A.V. Dediu Botezatu, M. Harja, Materials 15 (2022) 4657. https://doi.org/10.3390/ma15134657.
[26] W. Nyairo, J.B. Njewa, V.O. Shikuku, Front. Environ. Chem. 6 (2025) 1526366. https://doi.org/10.3389/fenvc.2025.1526366.
[27] J. Lach, E. Okoniewska, Molecules 29 (2024) 2418. https://doi.org/10.3390/molecules29112418.
[28] V.R. Kondakindi, R. Pabbati, P. Erukulla, N.R. Maddela, R. Prasad, Environ. Chem. Ecotoxicol. 6 (2024) 408-421. https://doi.org/10.1016/j.enceco.2024.05.002.
[29] C. Sutherland, B.S. Chittoo, Adv. Environ. Eng. Res. 5 (2024) 024. https://doi.org/10.21926/aeer.2404024.
[30] M.G. Fadl, Sci. Rep. 13 (2023) 1576. https://doi.org/10.1038/s41598-023-28655-4.

UPOREDNA BIOSORPCIJA OLOVA (II) PRIMENOM *Saccharomyces cerevisiae* I ALGINATNIH KUGLICA SA NANOUGLJENIKOM

ALAA A. BAHAT

WAFAA K. MAHMOOD

SAMAR S. HUSSEIN

Department of Mining and Extractive Metallurgy Engineering, College of Production Engineering and Metallurgy, University of Technology, Iraq

Uklanjanje Pb (II) iz vodenih rastvora ispitivano je primenom dva imobilisana sorbenta: alginatnih kuglica sa kvascem Saccharomyces cerevisiae i alginatnih kuglica sa nanougljenikom (višeslojnim ugljeničnim nanocevima). Kuglice koje su sadržale 0,6 ili 0,8 g sorbenta dovođene su u kontakt sa rastvorima Pb (II) nominalnih koncentracija 50, 100, 300 i 500 mg/L (koncentracije izmerene atomskom apsorpcionom spektrometrijom, AAS, iznosile su 58,1; 102,8; 323,0 i 496,0 mg/L). Alginatne kuglice sa kvascem pokazale su veću efikasnost pri nižim koncentracijama Pb (II), pri čemu je pri nominalnoj koncentraciji od 50 mg/L i sadržaju sorbenta od 0,8 g postignuto uklanjanje od 37,65% tokom prvih 5 min. Alginatne kuglice sa 0,8 g nanougljenika pokazale su najveći prividni sorpcioni kapacitet pri koncentraciji od 500 mg/L (45,76 mg/g), budući da ni nakon 60 min nije dostignut plato sorpcije. Kinetički model pseudo-drugog reda bolje je opisivao eksperimentalne podatke od modela pseudo-prvog reda u 8 od ukupno 12 nelinearnih prilagođavanja. Ovakav rezultat je u skladu sa pretpostavkom da je brzina procesa ograničena hemisorpcijom, ali sam po sebi ne predstavlja dokaz za takav mehanizam. Podaci dobijeni pri koncentraciji od 500 mg/L isključeni su iz modelovanja zbog nezadovoljavajućeg kvaliteta prilagođavanja modela ili fizički neutemeljenog tumačenja dobijenih parametara. U opsegu koncentracija od 50 do 300 mg/L, rezultati nelinearnog prilagođavanja pokazali su da Langmirov model bolje opisuje sorpciju kod alginatnih kuglica sa 0,6 g kvasca i 0,8 g nanougljenika, dok je Frojndlihov model bio pogodniji za kuglice sa 0,8 g kvasca i 0,6 g nanougljenika. Prema tome, očekivana promena odgovarajućeg modela sa povećanjem sadržaja sorbenta uočena je samo kod kuglica sa kvascem. Dobijeni rezultati ukazuju na to da su alginatne kuglice sa kvascem pogodnije za tretman vodenih rastvora sa nižim koncentracijama Pb (II), dok su alginatne kuglice sa nanougljenikom pogodnije za tretman rastvora sa višim koncentracijama ovog metala.

NAUČNI RAD

Ključne reči: adsorpcione izoterme; kinetika adsorpcije; biosorpcija; adsorpcija u zavisnosti od doze sorbenta; imobilisane kuglice.